Macromolecules
ARTICLE

Macromolecules **2009**, *42*, 8443–8450 **8443**
DOI: 10.1021/ma901423n

Sequence-Dependent Gelation Kinetics of β-Hairpin Peptide Hydrogels

Travis H. Larsen,[†] Monica C. Branco,[†] Karthikan Rajagopal,[‡] Joel P. Schneider,[‡] and Eric M. Furst*,[†]

[†]*Department of Chemical Engineering and Center for Molecular and Engineering Thermodynamics, University of Delaware, 150 Academy Street, Newark, Delaware 19716, and* [‡]*Department of Chemistry and Biochemistry, University of Delaware, Newark, Delaware 19716*

Received July 1, 2009; Revised Manuscript Received September 29, 2009

ABSTRACT: The gelation kinetics of four β-hairpin oligopeptides that have been designed to exhibit responsive behavior to changes in environmental conditions, such as pH, ionic strength and temperature, are characterized using multiple particle tracking microrheology and circular dichroism (CD) spectroscopy. The peptides, predominantly an alternating sequence of valine and lysine residues, differ by a point substitution of a single amino acid near a type II′ β-turn sequence. The rate of gelation becomes faster for point substitutions which reduce the total charge of the peptide. Similarly, increasing the ionic strength reduces or screens intra- and intermolecular electrostatic repulsions, again leading to faster gelation kinetics. CD measurements show that the concentration of folded peptide at the gel point decreases as the gelation kinetics become slower, possibly indicating a relationship between the assembly rate and the resulting gel microstructure. Finally, a model is developed based on the electrostatic barrier to peptide folding and association which agrees semiquantitatively with the microrheology results. This represents a first step toward understanding the role of peptide charge and physicochemical conditions in the self-assembly of these peptide hydrogelators.

Introduction

Self-assembling peptide-based hydrogels are an emerging class of biomaterials in which the material properties can be engineered through the amino acid sequence of individual peptide molecules.[1−3] Peptides can be designed to exhibit responsive behavior to environmental stimuli such as pH, temperature, ionic strength, cell culture media, and photoinitiation, making them ideal materials for biomedical applications.[3−7] These and other hydrogels are currently being developed for use in wound healing, drug delivery, and tissue engineering.[8−18] For such applications, the rate of hydrogel formation is often as important as the final bulk properties. For instance, it has been shown that a biocompatible hydrogel can serve as an artificial cellular matrix to promote tissue regeneration when formed in the gap of a severed tissue.[8−10] Suspending cells and growth factors into the injected solution can further improve the rate of recovery.[11] For this type of injectable delivery, a rapid liquid−solid transition upon injection is required to achieve a homogeneous suspension of cells and to ensure the localization of the treatment to the wound site to minimize undesired side effects. Hence, it is necessary to accurately characterize and compare the gelation kinetics of newly designed peptides to achieve desired rates of gelation under various environmental conditions.

In this work, we compare the gelation kinetics of four synthetic peptides.[4] The parent peptide, MAX1, is 20 residues, and consists of an alternating sequence of valines and lysines surrounding a tetrapeptide sequence with a high type II′ β-turn propensity.[5] In aqueous conditions, electrostatic repulsions between the positively charged lysine residues stabilize the molecules in an unstructured state. Folding and self-assembly is induced by changing the solution pH to reduce the point charge of the lysine residues, increasing the ionic strength to screen the electrostatic repulsions, or increasing the temperature to increase the attraction between hydrophobic residues. The folded peptide monomers are amphiphilic β-hairpins, which leads to the self-assembled structure of a network of physically cross-linked semiflexible filaments.[5,19] The peptides compared here are derivatives of MAX1, differing by a point substitution of the 15th residue, which replaces lysine (pK_a = 10.8) by either a threonine (neutral), glutamine (neutral), or glutamic acid (pK_a = 4.3). This single amino acid substitution near the turn sequence changes the electrostatic repulsive energy barrier required for *intra*molecular folding and *inter*molecular assembly, which should consequently alter the rate of self-assembly and gelation. An overview of the self-assembly and a summary of the sequences and overall charge of each peptide are given in Figure1.

During filament assembly, the peptide monomers undergo a conformational change from an unassociated state with predominantly random-coil content to an associated one with predominantly β-sheet content. This change in secondary and tertiary structure can be monitored using circular dichroism (CD) spectroscopy. These measurements are able to provide some insight into the kinetics of assembly by tracking the rate of increase in β-sheet content and consequent decrease in random-coil content. However, the relationship between the folding event, incorporation of the peptide into growing filaments, and formation of an elastic network is poorly understood and not resolvable using CD spectroscopy alone.[20]

Multiple particle tracking microrheology is used to directly monitor the kinetics of gelation. Microrheology is ideally suited for studying soft materials, especially weak gelators as they undergo a time-dependent liquid-to-solid transition.[21,22] Bulk rheology experiments for 2 wt % MAX1 gels show that the elastic component of the complex modulus exceeds the viscous component at the earliest measurable times.[4,19] For self-assembling systems, the concentration can be reduced to slow the kinetics of assembly, but this results in low modulus gels that are below the reliable detection limits of the rheometer. In contrast, multiple

*Corresponding author. E-mail: furst@udel.edu.

Published on Web 10/19/2009

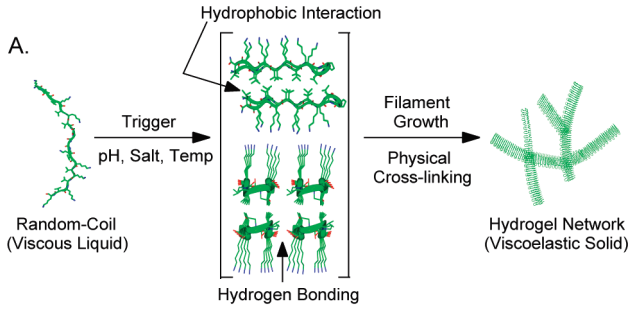

Figure 1. (A) Peptide folding and self-assembly mechanism. The dimensions of a single folded β-hairpin peptide monomer are 3.15 × 0.47 × 1.0 nm. (B) Sequences and overall net charge of the peptides investigated in this study.

particle tracking microrheology not only benefits from high sensitivity to changes in viscoelastic properties at low moduli, but also the ability to take quick measurements (~30 s) over 2−3 decades of time scales for a system in which the moduli are changing fairly rapidly with time. This latter aspect enables time-cure superposition analysis.[21,30] The technique is also a passive technique that applies no external forces, so the fragile growing structures do not risk being affected by the measurement. Finally, only small sample volumes are required (50 μL), which makes it possible to investigate the rheological properties of scarce materials. In this work, we will employ both CD spectroscopy and multiple particle tracking to compare the gelation kinetics of the four peptides and attempt to bridge a relationship between the rate of β-sheet structure formation to that of network assembly. The gelation kinetics are compared to a lumped model of the electrostatic interactions between peptides in order to provide a preliminary understanding of the combined effects of changes to the ionic strength, temperature, and introduction of amino acid substitutions.

Experimental Section

Sample Preparation. The peptides used in this study are made using an Fmoc-based solid-phase synthesis. They are purified by reverse phase HPLC and lyophilized for storage. The procedure has been described in detail previously.[5] Peptide stock solutions are prepared immediately prior to each experiment by redispersing lyophilized peptide in ultrapure water (resistivity 18.2 MΩ·cm). The gelation process is initiated by changing the environmental conditions (i.e., ionic strength) with the addition of buffer.

The tracer particles used in the microrheology experiments are fluorescent polystyrene microspheres with diameter $2a$ = 1.05 ± 0.01 μm (Polysciences, Warrington, PA). Particles are washed three times with ultrapure water and then sonicated for 15 min to break up possible aggregates. They are added to a final concentration of 0.15 vol. % before gelation is initiated. This particle concentration is chosen to achieve adequate tracking statistics, but does not influence the observed gelation kinetics. (See Supporting Information) In previous work, we have shown the probe particle surface chemistry does not affect our measurements and that microrheology results compare well with bulk rheology.[20]

Multiple Particle Tracking Microrheology. The experimental procedure has been reported previously.[21] Briefly, immediately after gelation is initiated by the addition of buffer, sample solutions are introduced into rectangular capillary cells (0.20 × 2.00 × 50 mm, Vitrotubes, Vitrocom), which serve as sample chambers. Excess air is removed and the cells are sealed to a microscope slide with fast-curing UV epoxy (Norland Products, NOA 81). Samples are transferred to the microscope and data are collected at discrete time points during the gelation process.

Samples were imaged and captured using two different experimental setups. *Equipment Setup No. 1*: The embedded tracer particles are imaged at a total magnification of 63× using an inverted epifluorescence microscope (N.A. 1.2, 63× water-immersion objective, 1.0× tube lens, Axiovert 200, Zeiss). The motion of ~150 in-frame particles is captured at 30 Hz with an exposure time of, σ = 1 ms, for a total of 800 frames with a CMOS high-speed camera (Phantom v5.1, Vision Research). *Equipment Setup No. 2*: Probe particles are imaged at a total magnification of 64× (N.A. 0.75, 40× air objective, 1.6× tube lens, Axiovert 200, Zeiss). Particle motion is recorded for ~120 in-frame particles at 60 Hz with anexposure time of, σ = 16.7 ms, for 500 frames using a CCD camera (UP-680CL, Uniq Vision). The effect of these equipment differences on the observed measurement error is discussed in the Supporting Information. For all experiments, particles are tracked using a weighted centroid method developed for the IDL language (ITT Visual Information Solutions, Boulder, CO).[23] The ensemble-averaged mean-squared displacement (MSD), $\langle \Delta r^2(\tau) \rangle$, is calculated from the particle trajectories.

Circular Dichroism (CD). Samples are prepared as described above, without the addition of tracer particles, and loaded into a water-jacketed quartz sample chamber for temperature control. The gels that form in the sample chamber are transparent and control experiments (provided in the Supporting Information) verify that the absence or presence of the tracers have no effect on the measured results. CD spectra are collected using a J-810 spectropolarimeter (Jasco, Tokyo, Japan). The mean residue ellipticity $[\theta]$ is calculated as $[\theta] = \theta_{obs}/(10lcr)$, where θ_{obs} is the measured ellipticity (mdeg), l is the cell length in centimeters, c is the peptide concentration in molarity (mol/liter), and r is the number of residues per peptide. The existence of β-sheet secondary structure for the peptides is characterized by a minimum in $[\theta]$ at a wavelength of λ = 216 nm. Exact concentrations are verified using a UV−vis spectrophotometer to measure absorbance at 220 nm (molar absorption coefficient, ε = 15750 cm^{-1} M^{-1}).[4]

Results and Discussion

Microrheology of the Gel Transition. *Mean-Squared Displacement*. Previously, we presented an analysis of microrheological data taken through the gel transition for the MAX1 and MAX1(K15T) peptides.[20−22] The probe particle dynamics are interpreted in terms of the viscoelastic properites of the material using the generalized Stokes−Einstein relation

$$\langle \Delta r^2(t) \rangle = \frac{k_B T}{\pi a} J(t) \tag{1}$$

where $J(t)$ is the creep compliance, a is the radius of the probe particles and k_BT is the thermal energy.[24−26] $J(t)$ relates the material strain deformation $\gamma(t)$ to the rate of applied stress $\dot{\sigma}(t)$ by the equation $\gamma(t) = \int_0^t J(t-t')\dot{\sigma}(t)\,dt'$.[27] The critical gel point is reached when the network percolates the sample-space to form an infinite polymer molecule. At the gel point, the MSD and creep compliance exhibit power-law behavior over all times

$$J_c(t) = \frac{\sin n\pi}{n\pi S} t^n \tag{2}$$

where S is the gel strength with units Pa·s^n and n is the critical relaxation exponent.[28,29]

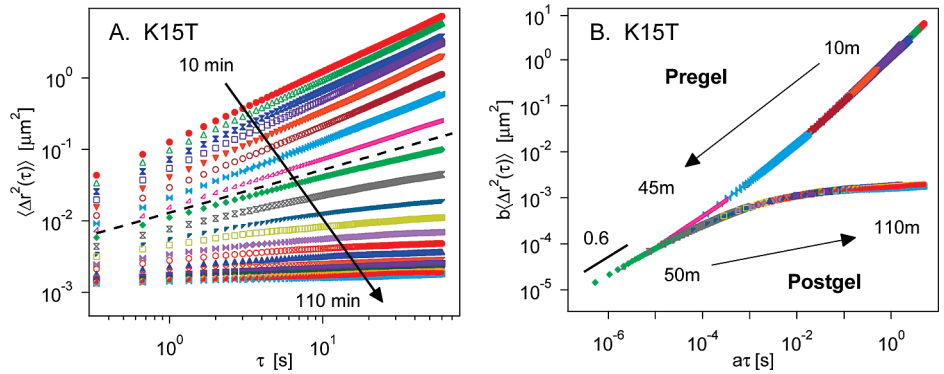

Figure 2. (A) Ensemble averaged mean-squared displacement $\langle \Delta r^2(\tau) \rangle$ of polystyrene microspheres ($2a = 1.05 \pm 0.01\ \mu$m) embedded in 0.15 wt % self-assembling MAX1(K15T) peptide. (pH 8.5, 50 mM BTP, 25 mM NaCl, $T = 25$ °C) Individual curves represent the particle dynamics at various times between 10 and 110 min after gelation is initiated by the addition of buffer. (B) Superposition of the mean-squared displacements before and after the sol−gel transition. The converging master curves have a terminal logarithmic slope of $\alpha = 0.6$ at the critical gel point, identifying the critical relaxation exponent n.

Figure 2A shows one such gelation experiment and the typical mean-squared displacement curves taken at increasing times after peptide self-assembly is initiated. The data shown are for 0.15 wt % MAX1(K15T) (pH 8.5, 50 mM BTP, 25 mM NaCl, $T = 25$ °C), acquired using Equipment Setup No. 1. Here, lag time τ is the time over which the MSD is calculated, which should not be confused with the time after the initiation of the gelation reaction.

Using time-cure superposition,[21,30] master curves are constructed before and after the gel point by multiplying the lag time and mean-squared displacement by shift factors a and b, respectively, as shown in Figure 2B. These shift factors are related to the longest relaxation time and steady-state creep compliance, and when plotted as a function of time after the gelation reaction is initiated,[21] diverge at the critical gel time, $t_c = 47.5$ min (data not shown). The critical gel point can also be estimated between the time of the last MSD curve to successfully scale onto the pregel curve and time of the first postgel curve. The critical relaxation exponent n is then identified as the logarithmic slope, $n = \alpha \equiv d[\log\langle \Delta r^2(\tau) \rangle]/d[\log \tau]$, of the converged master curves at the shortest scaled lag times. In this case, the pregel and postgel master curves both converge to a logarithmic slope of $\alpha \approx 0.6$.

The value of the critical exponent, $n \approx 0.6$, is in agreement with those predicted for fractal-like polymer growth, where the values of n can range between 0.55 and 0.7 depending on the fractal dimension and degree of hydrodynamic screening. This growth mechanism is expected for self-assembly of the filamentous peptide network, and the value of $n \approx 0.6$ is assumed to be conserved for all of the peptide systems over the range of gelation kinetics studied. Therefore, it is possible to define the gel point by the value of the logarithmic slope of the mean-squared displacement at long lag times. This is necessary when static or dynamic errors in the particle tracking[31] limit the accuracy of the MSD at short lag times, which prevents an accurate shifting of the data into master curves, as discussed in the Supporting Information. In this work, we determine the logarithmic slope of the MSD from the last decade of lag times, typically $\tau > 1$ s. Figure 3 plots the logarithmic slope as a function of time, and the critical gel time, $t_c = 47.5$ min, can be determined as the time at which $\alpha = 0.6$, shown by the intersection with the solid black line. The dashed lines indicate the possible theoretical range of the critical relaxation exponent.[20]

Comparison of Peptide Kinetics. With a reliable method for determining the gel point established, we next discuss the sequence-dependent gelation kinetics of the peptides. We

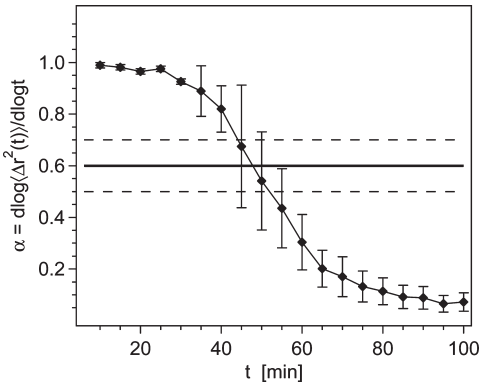

Figure 3. Logarithmic derivative of the MSD, α, calculated from the data in Figure 2 and plotted as a function of time after the initiation of gelation of MAX1(K15T) peptide. The solid line indicates the predicted value of α at the critical gel point, while the dashed lines represent the theoretical limits. The time at which $\alpha = 0.6$ is the critical gel point. In this case, $t_c = 47.5$ min.

were unable to identify a single set of conditions in which self-assembly were favorable for all four peptides over reasonable time periods for microrheological measurements (concentration, pH, ionic strength, temperature); therefore, we altered the environmental conditions for each peptide to gel at similar times. We then use our knowledge of how these conditions affect the energetics of assembly to compare the relative gelation kinetics between the peptides.

Ionic Strength. Electrostatic repulsion between positively charged lysine residues stabilize the peptides in a random coil or unfolded state at low pH, temperature, and ionic strength. By increasing the concentration of monovalent salt, these repulsive interactions are screened, making folding and self-assembly favorable. Figure 4A plots the logarithmic slope of the MSD, α, versus time for the four peptides. In these experiments, the salt concentration is varied to achieve similar gelation kinetics, while all other conditions are held constant (0.15 wt % peptide, pH 8.5, 50 mM BTP, $T = 25$ °C). The gel point is determined by the time at which $\alpha = 0.6$, as indicated by the intersection with the solid black line. In the absence of salt, MAX1(K15E) gels rapidly under these conditions, with a gel point of $t_c = 9 \pm 1$ min. The gelation of MAX1(K15T) and MAX1(K15Q) occur at much slower rates without salt (not shown), but the addition of 50 mM NaCl decreases the gel point to a time of $t_c = 21 \pm 1$ min and $t_c = 26 \pm 2$ min, respectively. Finally, at the highest salt concentration of 100 mM NaCl, MAX1 gels at $t_c = 94 \pm 7$ min.

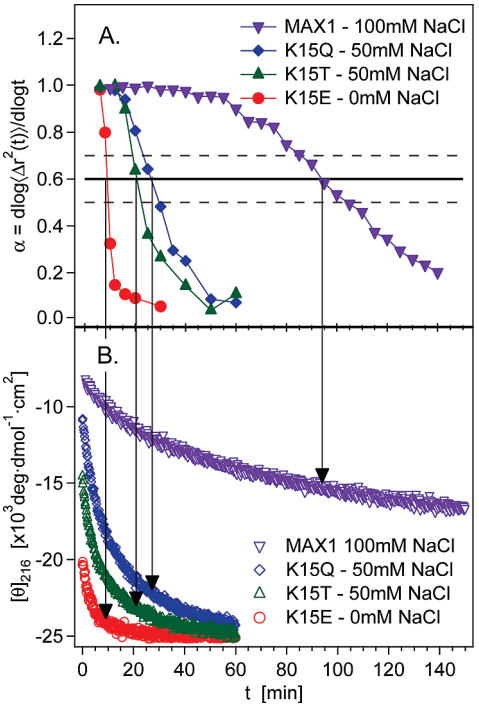

Figure 4. Effect of ionic strength on the gelation kinetics. (A) MSD logarithmic slope, α, plotted as a function of time for the four peptides at different ionic strengths (0.15 wt % peptide, pH 8.5, 50 mM BTP, $T = 25$ °C). The logarithmic slope is calculated for the past decade of lag times, typically $\tau > 1$ s, of the MSD. (B) CD spectroscopy shows the ionic strength dependence of β-sheet content.

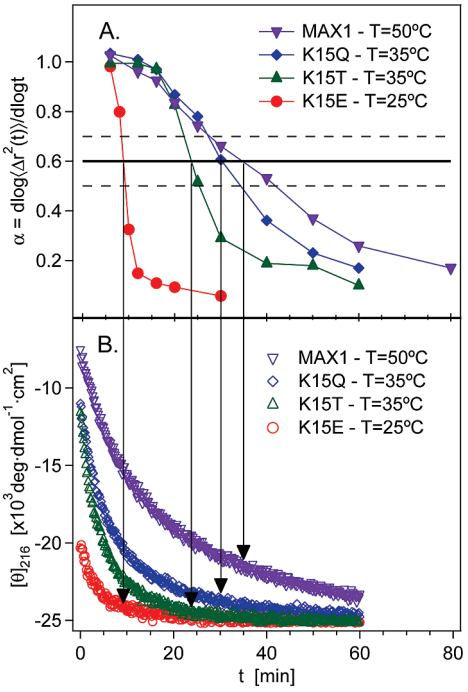

Figure 5. Effect of temperature on the gelation kinetics. (A) MSD logarithmic slope, α, plotted as a function of time for the four peptides at different temperatures (0.15 wt % peptide, pH 8.5, 50 mM BTP, 0 mM NaCl). (B) CD spectroscopy shows the temperature dependence of β-sheet content.

These results can be explained by the relative overall charge of each peptide. MAX1(K15E) has a net charge of +7, which is the lowest positive charge of the peptides studied. The glutamic acid residue, which is negatively charged at this pH, may also produce a cross strand salt bridge, which further promotes folding and self-assembly of the peptide. Thus, even without the addition of a monovalent salt, MAX1(K15E) gels more rapidly than the other peptides. MAX1(K15T) and MAX1(K15Q) both have point substitutions incorporating a neutral amino acid, resulting in a net charge of +8 and similar overall kinetics. With a higher total peptide charge, a substantial amount of salt is required to achieve gelation rates similar to MAX1(K15E). MAX1 has the highest net charge (+9), which requires the most screening to induce gelation. Even at this high salt concentration, MAX1 exhibits the slowest gelation kinetics. Higher concentrations of salt could not be tested due to aggregation of the embedded tracer particles.

Temperature. The peptides are primarily composed of alternating lysine and valine residues. In the folded state, the peptides form an amphiphilic molecule with a hydrophilic (lysine) and hydrophobic (valine) face. The association energy of the hydrophobic faces depends on temperature. Increasing the temperature increases the hydrophobic effect, and is expected to increase the rate of self-assembly.[32] Higher temperatures also increase the probability of crossing the repulsive electrostatic barrier. Figure 5A shows the logarithmic slope of the MSD, α, versus time for the four peptides. For these experiments, the temperature is varied, while all other conditions remain constant (0.15 wt % peptide, pH 8.5, 50 mM BTP, 0 mM NaCl). MAX1(K15E) is at identical conditions as shown in Figure 4A, and has a gel point of $t_c = 9 \pm 1$ min at $T = 25$ °C. To increase the assembly rate of MAX1(K15T) and MAX1(K15Q), the temperature is increased to $T = 35$ °C, resulting in gel points of $t_c = 24 \pm 2$ min and $t_c = 30 \pm 2$ min, respectively. Further increasing the temperature up to $T = 50$ °C, results in MAX1 reaching the critical gel point at $t_c = 35 \pm 2$ min. Because the peptides have the same number of hydrophobic valine residues, the difference in assembly kinetics at a given temperature is still primarily attributable to the total charge of the peptides. The rapid folding and assembly of MAX1(K15E) is a result of the lower energetic barrier due to the presence of the negatively charged glutamic acid, as explained above, which again leads to the fastest gelation kinetics, even at room temperature. MAX1(K15T) and MAX1(K15Q) are expected to gel at a similar rate to each other, but slower than MAX1(K15E) at a given temperature based on the total charge of these peptides. However, at a higher temperature of $T = 35$ °C, the increased thermal energy drives the hydrophobic effect and increases the probability of overcoming an energetic barrier to association, allowing the peptides to assemble at faster rates. MAX1 has the greatest repulsive energy barrier to overcome, and it therefore requires the highest temperature in order to gel at a similar rate as the other peptides.

Circular Dichroism. The sequence-dependent kinetics of folding and self-assembly of the four peptides are further investigated using CD spectroscopy. The existence of β-sheet secondary structure is detected by a minimum in the mean-residue ellipticity, $[\theta]$, at a wavelength of $\lambda = 216$ nm.[20] Figure 4B and Figure 5B plot $[\theta]_{216}$ as a function of time after gelation is initiated. For all curves, $[\theta]_{216}$ decreases continuously with time, corresponding to an increasing presence of β-sheet. At short times, the rate of β-sheet formation is very rapid, while at long times the magnitude of $[\theta]_{216}$ slowly converges to a common value, indicating the completion of the β-sheet transformation. The time required for the evolution of the β-sheet structure is shortest for MAX1(K15E), intermediate for MAX1(K15T) and MAX1(K15Q), and longest for MAX1.

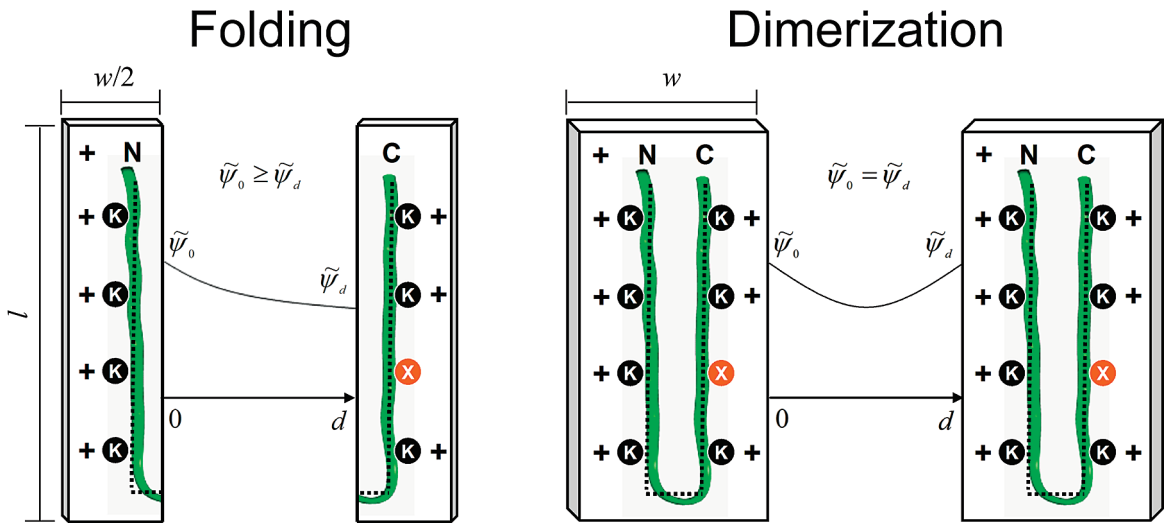

Figure 6. Model of the electrostatic interaction potential for peptide folding and self-assembly. In both cases, the geometry is simplified by considering two parallel plates, where the dimensions ($l \times w \times t$) of a single β- hairpin peptide monomer are $3.15 \times 0.47 \times 1.0$ nm. For peptides other than MAX1 (which has a lysine at the 15th residue position), the folding event is modeled as the interaction between two plates with dissimilar charge, while dimerization is always modeled as two similarly charged plates.

The gelation process is dependent on the conformational state of the peptide. One hypothesis is that peptide monomers fold into β-hairpins as they are recruited into the self-assembling filaments. The growth and physical cross-linking of filaments ultimately forms the microstructure of the gel network. Therefore, a direct relationship exists between the extent of β-sheet content and the extent of network formation during gelation. CD spectroscopy and microrheology provide complementary insight into the gelation mechanism of these materials. CD spectroscopy can monitor the extent of β-sheet in the system, but is unable to differentiate between folded monomers and those associated into the network, which makes the measurements potentially insensitive to network growth. Microrheology can measure changes in the viscoelastic properties of the fluid by the formation of structure, but is otherwise insensitive to the folded state of the peptides.

Comparing the CD and particle tracking results in Figure 4 and Figure 5, we use arrows to indicate the values of $[\theta]_{216}$ at the critical gel point. We find that the value of $[\theta]_{216}$ at t_c is greater for slower forming gels. This possibly indicates that the rate of folding is faster than the rate of self-assembly for the faster gelators, resulting in an excess of free β-hairpin monomers at the gel point. More likely, however, the self-assembly process is more efficient for slower kinetics, resulting in long filaments with fewer interfilament cross-links, which are thought to form via facial association defects during self-assembly. The growth of long, loosely cross-linked filaments requires fewer folded monomers to form a percolated network and results in a less rigid gel than a network formed via percolation of tightly cross-linked filament clusters. These observations are in agreement with recent comparisons of CD and bulk rheology data, which show that upon complete conversion of available peptide to β-sheet, fast-forming MAX1(K15E) yields a gel with a higher elastic modulus than slow-forming MAX1.[1]

Electrostatic Model of the Gelation Kinetics. Gelation of the MAX1 peptide and its variations are sensitive to single amino acid substitutions at the 15th residue position. We hypothesize that the changes in the intra- and intermolecular electrostatic interactions limit the rate of self-assembly, and hence, the gelation kinetics. Here, we present a simplified electrostatic double layer model to test this hypothesis. The model provides a qualitative understanding of the experimental trends and a semiquantitative estimate of the relative gelation times as a function of ionic strength and temperature as point substitutions are made in the amino acid sequence.

Peptide Structure. Earlier work[19] demonstrated that the gel microstructure is composed of filaments, which presumably form via the addition of folded peptide monomers to terminal ends of the growing structure, as summarized in Figure 1. Self-assembly may depend on both the interaction potential of the folding event, the energy required for the two arms of a single peptide molecule to come together, and the interaction potential of dimerization, the energy required for two separate monomers to approach close enough to associate. For both cases, we assume a simplified geometry of two parallel plates, as shown in Figure 6. The size of the plates are determined by the dimensions of the folded monomer, with length $l = 3.15$, width $w = 0.47$, and thickness $t = 1.0$ nm. For folding, we model the interaction of two plates of dissimilar charge, each with surface area, $s_i = 0.74$ nm^2. One branch of the peptide has four positively charged lysine residues and the N-terminal amine, while the other branch has three lysines and one amino acid that varies between the peptides between lysine, glutamine, glutamic acid, and threonine. The charge of this substituted amino acid affects the overall charge of the second branch and therefore the interaction potential between the two branches. For dimerization, the interaction is modeled as two plates of equal charge and area, $s_d = 1.48$ nm^2. Once again, the total charge of the interacting surfaces, as well as the corresponding interaction potential, is determined by the amino acid substitution.

Surface Charge and Potential. The peptides studied in this paper have been engineered to self-assemble upon changes in ionic strength and temperature. The pH determines the charged state of the lysine ($pK_a = 10.8$) residues, the substituted glutamic acid ($pK_a = 4.3$) residue in MAX1(K15E), and the free amine group of the N-terminus ($pK_a = 7.8$), while the ionic strength affects the degree of screening between the charges. As the pH increases above 7, the glutamic acid carries a negative charge, while the lysines and free amine partially deprotonate, decreasing the overall charge density of the molecules. The surface charge density, σ, and electrostatic potential at the peptide surface, ψ_s, can be expressed in

terms of the dependence of these values on the protonization state of the ionizable residues: lysine (K), glutamic acid (E), and the free amine of the N-terminus (n)

$$\sigma = \frac{-\sigma_{\mathrm{E}}^{\max} 10^{\mathrm{pH}-\mathrm{p}K_{\mathrm{E}}}}{e^{-\tilde{\psi}_s} + 10^{\mathrm{pH}-\mathrm{p}K_{\mathrm{E}}}} + \frac{\sigma_{K}^{\max} e^{-\tilde{\psi}_s}}{e^{-\tilde{\psi}_s} + 10^{\mathrm{pH}-\mathrm{p}K_{\mathrm{K}}}} + \frac{\sigma_{\mathrm{n}}^{\max} e^{-\tilde{\psi}_s}}{e^{-\tilde{\psi}_s} + 10^{\mathrm{pH}-\mathrm{p}K_{\mathrm{n}}}} \quad (3)$$

where e is the charge of an electron, $\tilde{\psi}_s = e\psi_s/(k_{\mathrm{B}}T)$ is the scaled electrostatic potential at the surface, and $\sigma^{max} = en/s$ is the maximum surface charge density, with n/s being the surface density of the ionizable residue.[2,33] This equation as written is valid for MAX1(K15E), while only the second and third terms on the right side of the equation are necessary for MAX1(K15T), MAX1(K15Q), and MAX1, since the only ionizable residues in these peptides are lysines and the free amine at the N-terminus. The Grahamme equation relates σ and ψ_s,[34]

$$\sigma = \frac{2\varepsilon\varepsilon_0\kappa k_{\mathrm{B}}T}{e}\sinh(\tilde{\psi}_s/2) \quad (4)$$

where ε is the dielectric constant of water, ε_0 is the vacuum permittivity, and

$$\kappa = \sqrt{2e^2c/(\varepsilon\varepsilon_0 k_{\mathrm{B}}T)}$$

is the Debye−Hückel parameter, or inverse Debye length.[34] The effect of salt screening is accounted for in this model by κ, which is a function of the bulk ion concentration, and scales as $\kappa \sim c^{1/2}$. In this case, when only monovalent salts are considered, **c** denotes the total salt concentration. In our model, we assume c to be the concentration of the anions present in our samples, such that $c = [\mathrm{OH}^-] + [\mathrm{TFA}^-] + [\mathrm{Cl}^-] + [\mathrm{BTP}^-]$, where $[\mathrm{TFA}^-]$ is the concentration of TFA that remains bound to the peptide during synthesis, which is assumed to be equal to the number of lysine and N-terminal free amine residues. $[\mathrm{BTP}^-]$ is the concentration of the zwitterionic bis-tris propane (BTP) buffer that is deprotonated, and $[\mathrm{Cl}^-]$ is the concentration of chloride ions present in solution from both the addition of HCl, which is added to adjust the solution to the appropriate pH, and the addition of NaCl, which acts as the variable for increasing the total ionic strength between samples.

The calculated surface charge density (solid lines) and electrostatic potential at the surface (dashed lines) are plotted in Figure 7 as a function of pH. For MAX1(K15E), we observe a decrease in σ and ψ_s at low pH, indicating that the glutamic acid residue is negatively charged. For all peptides, these values continue to decrease for pH > 6.5 as the lysine residues are deprotonated and become neutralized. This behavior agrees well with the lack of self-assembly observed experimentally for all peptides, except MAX1-(K15E), at pH below approximately 6.5 at these temperatures and ionic strengths. Note also that MAX1(K15E) becomes negatively charged for pH > 11.5, at which point the glutamic acid residue is the only charged group. The black, vertical dashed line indicates pH 8.5, the pH at which our samples are studied. At this pH, repulsive interactions are still present for all peptides, which act to slow down the gelation kinetics for experimental measurement.

Interaction Potential. With the surface charge densities and electrostatic potentials determined for the peptide, we next calculate intra- and intermolecular interaction potentials related to the kinetics of peptide association.

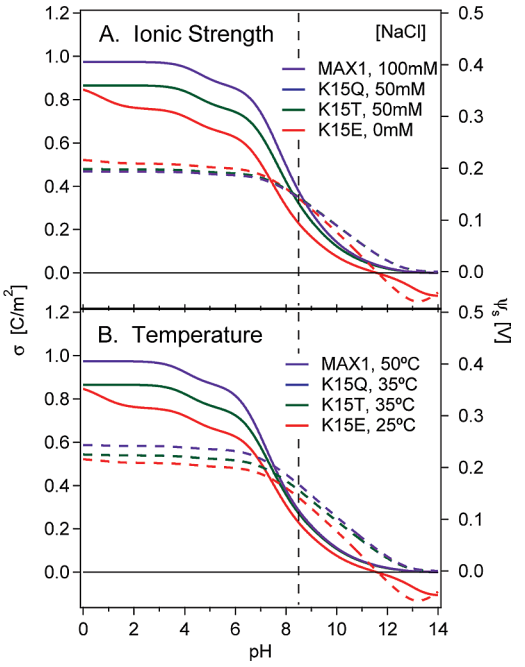

Figure 7. Surface charge density (solid lines) and electrostatic potential at the surface (dashed lines) as a function of pH for the four peptides at varying (A) ionic strength and (B) temperature (0.15 wt % peptide, 50 mM BTP).

As discussed above, our coarse-grained model treats the peptide as a solid volume with flat interfaces.

We begin with the electrostatic interactions. The interaction potential of plane parallel double layers has been solved exactly by Verwey and Overbeek and Devereux and de Bruyn.[35,36] These solutions include elliptical integrals, which has motivated the calculation of approximate expressions using Taylor series expansions. We use approximate solutions determined by Zhang,[37−39] which converge quickly, are applicable over a large range of electrostatic potentials, and agree well with the exact solutions found by Devereux and de Bruyn.

We model the interaction between the two peptide branches using expressions for two plates of the same sign but dissimilar charge density.[38] For the special case in which MAX1(K15E) becomes negatively charged for pH > 11.5, expressions for two plates of opposite sign and dissimilar charge density are used to model this interaction.[39] Then, to account for the electrostatic barrier between two peptide molecules, we use expressions for two plates of the same sign and charge density.[37] Because the exact equations are long, we have not reproduced them here; instead, the reader should refer to the original texts.[37−39]

In Figure 8, we show the intramolecular $U_i = W_i s_i$ and intermolecular $U_d = W_d s_d$ electrostatic repulsion as a function of separation d and scaled by the thermal energy $k_{\mathrm{B}}T$, where s_i and s_d are the corresponding areas ofthe peptide faces. The calculated repulsion decreases as the total charge on the peptide is reduced. This correlates with the decreasing gelation time observed experimentally from MAX1 (total charge +9) to MAX1(K15E) (total charge +7), even with decreasing ionic strength and less screening of the charges. Both repulsions are significant in magnitude relative to thermal energy; however, the electrostatic interactions corresponding to the *inter*molecular repulsion is larger than the corresponding intramolecular repulsion between the two branches of the same peptide. Therefore, we will use the assembly of two monomers as the rate limiting step of the self-assembly and gelation kinetics.

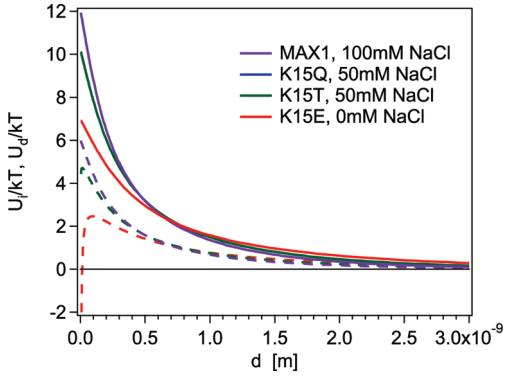

Figure 8. Calculated interaction energies of the peptide intramolecular U_i (dashed lines) and intermolecular U_d (solid lines) screened electrostatic interactions.

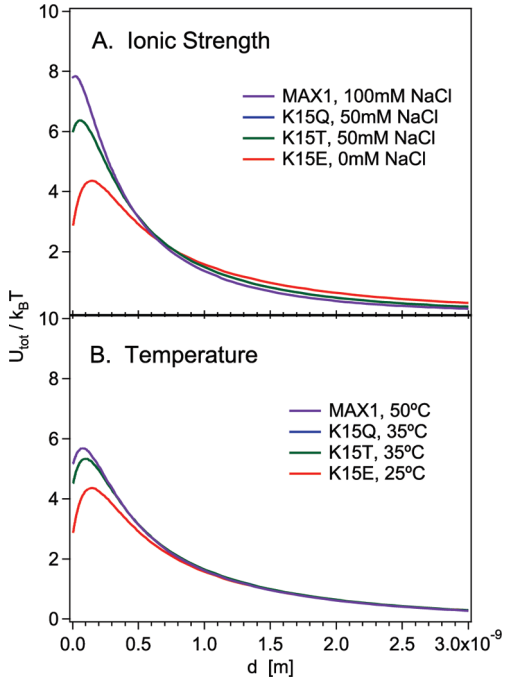

Figure 9. Total dimensionless interaction potential as a function of separation distance for the four peptides at varying (A) ionic strength and (B) temperature (0.15 wt % peptide, pH 8.5, 50 mM BTP).

Lastly, the large number of hydrophobic residues suggests that the hydrophobic interaction is the dominant attractive interaction between peptides, although van der Waals interactions and hydrogen bonding are also likely to play a role in the self-assembly of these materials. We include the hydrophobic interaction between surfaces using the expression[34]

$$W_h = -2\gamma e^{-d/\lambda_0} \tag{5}$$

where γ is the surface energy per unit area and λ_0 is the characteristic range of the attraction. Combining the screened electrostatic repulsion and the hydrophobic attraction, the total interaction energy is

$$U_{tot} = (W_d + W_h)s_d \tag{6}$$

As shown in Figure 9, the inclusion of the hydrophobic interaction significantly reduces the magnitude of the electrostatic repulsive barrier when compared to Figure 8.

Table 1. Gelation Times of Peptide Sequences Relative to the Gel Time of MAX1 at 100 mM NaCl and 25 °C Calculated Using the Electrostatic Model and Compared to the Experimental Gel Times

peptide	[NaCl] (mM)	temp (°C)	model t_c' (min)	experiment t_c (min)
MAX1	100	25		94 ± 7
MAX1(K15T)	50	25	23	21 ± 1
MAX1(K15Q)	50	25	23	26 ± 2
MAX1(K15E)	0	25	3	9 ± 1
MAX1	0	50	12	35 ± 2
MAX1(K15T)	0	35	8	24 ± 2
MAX1(K15Q)	0	35	8	30 ± 2

Estimate of Gelation Time. With the total interaction potential calculated as a function of temperature and ionic strength, we now estimate the gelation times of the peptides relative to the "native" MAX1 peptide. We assume that the gelation time is proportional to the energetic barrier each monomer needs to cross before joining the growing structure. This sets the characteristic time for self-assembly and gelation, and can be written[40]

$$t_c' \propto t_B e^{U_{\max}/k_B T} \tag{7}$$

where $U_{\max}$ is the maximum of the total energy U_{tot} and $t_B = 3\eta_0/4k_BT\nu$ is the time scale for Brownian diffusion of the molecule. Here, $\eta_0 \approx 1$ mPa·s is the initial viscosity of unfolded peptide monomer dissolved in water, and ν is the number density of β-hairpin monomers.

Using the gel time of MAX1 at 100 mM NaCl and 25 °C, $t_{c,\text{MAX1}} = 94$ min, as a reference, each gel time relative to $t_{c,\text{MAX1}}$ is then calculated by the ratio of the values t_c' given by eq 7. For the hydrophobic attraction, we find the best agreement between the model and experiment for the parameter values $\gamma = 6$ mJ/m^2 and $\lambda_0 = 0.1$ nm, which are in reasonable agreement with literature values.[34] The results are summarized in Table 1. With respect to experiments performed at the same temperature (25 °C), the model captures the dependence of the gel time on ionic strength and charge density. Point substitutions that eliminate one charge at the 15th residue position (MAX1(K15T) and MAX1(K15Q)) lead to faster gel times, even as the ionic strength, and hence screening of the electrostatic repulsion, is reduced. When the residue is substituted by one carrying a negative charge, as it is for MAX1(K15E), the average charge density of the peptide is further reduced. However, the model slightly under-predicts the gel time (3 min instead of the experimental time of 9 min.)

Next, we examine the effect of temperature. In this case, the model qualitatively captures the increase in the rate of gelation as the temperature increases, but quantitatively predicts faster kinetics than are observed experimentally. For instance, the calculated gel time of MAX1 for 0 mM NaCl and 50 °C is roughly three times faster (12 min) than the experimental value (35 min). The calculated gel times for peptides MAX1(K15Q) and MAX1(K15T) at 35 °C and MAX1(K15E) at 25 °C show an identical factor difference from the experimental values.

Overall, the gelation times predicted by the "lumped model" agree within an order of magnitude of those measured experimentally. While the model is only semiquantitative, it does qualitatively capture the dependence on combined changes in the ionic strength, temperature and point substitutions, such that the energy barrier required for self-assembly decreases as the total charge of the peptide decreases. While this provides a measure of confidence toward validating the empirical observations of the gelation

kinetics of the different peptides reported in this work, the complete kinetic pathway and potentially competing rates of peptide folding and association are almost certainly more complicated[41] and warrant further modeling.

Conclusions

Multiple particle tracking microrheology and circular dichroism were used to compare the gelation kinetics of four peptide hydrogelators. The gel point was defined as the time when the slope of the logarithmic slope of the mean-squared displacement curves, α, was equal to the critical relaxation exponent, $n \approx 0.6$. The gel point serves as a reference point by which to compare the peptides under various environmental conditions. It was shown that the rate of gelation can be controlled through careful design of the peptide sequence, which is vitally important for therapeutic applications, especially for injectable tissue scaffolds in wound healing. Furthermore, CD measurements demonstrated that the amount of associated peptide required to form a percolated network decreases as the gelation kinetics are slowed. This provides insight into the gel microstructure, possibly indicating that filament length increases while cross-linking density decreases when the assembly rates are slowed. Finally, a model was developed based on the electrostatic barrier to folding and association, which agreed semiquantitatively with the microrheology results, and accurately predicted that the rate of assembly increases as the total positive charge of the peptide decreases. In all, this represents a first step toward rationally engineering peptide sequences to control self-assembly and subsequent gelation for therapeutic applications.

Acknowledgment. We thank C. Roberts for helpful discussions. Funding for this work was provided by the National Institutes of Health (1 R01 EB003172-01 and 2 P20 016472-04), the National Science Foundation (CHE0348323) and the Procter and Gamble Company. E.M.F. also thanks the EU Erasmus Mundus and Eurheo programs for financial support.

Supporting Information Available: The effect of static and dynamic particle tracking error on the accuracy of the calculated MSD at short lag times, and its implications for the microrheology, is discussed in further detail. We also present control experiments showing that the probe particles do not affect the gelation or folding kinetics measured using microrheology and circular dichroism, respectively. This material is available free of charge via the Internet at http://pubs.acs.org.

References and Notes

(1) Haines-Butterick, L.; Rajagopal, K.; Branco, M.; Salick, D.; Rughani, R.; Pilarz, M.; Lamm, M. S.; Pochan, D. J.; Schneider, J. P. *Proc. Natl. Acad. Sci. U.S.A.* **2007**, *104*, 7791–7796.
(2) Savin, T.; Doyle, P. S. *Soft Matter* **2007**, *3*, 1194–1202.
(3) Ozbas, B.; Kretsinger, J.; Rajagopal, J.; Karthikanand Schneider; Pochan, D. *Macromolecules* **2004**, *37*, 7331–7337.
(4) Schneider, J.; Pochan, D.; Ozbas, B.; Rajagopal, K.; Pakstis, L.; Kretsinger, J. *J. Am. Chem. Soc.* **2002**, *124*, 15030–15037.
(5) Pochan, D.; Schneider, J.; Kretsinger, J.; Ozbas, B.; Rajagopal, K.; Haines, L. *J. Am. Chem. Soc.* **2003**, *125*, 11802–11803.
(6) Kretsinger, J.; Haines, L.; Ozbas, B.; Pochan, D.; Schneider, J. *Biomaterials* **2005**, *26*, 5177.
(7) Haines, L. A.; Rajagopal, K.; Ozbas, B.; Salick, D. A.; Pochan, D.; Schneider, J. *J. Am. Chem. Soc.* **2005**, *127*, 17025–17029.
(8) Ellis-Behnke, R. G.; Liang, Y.-X.; You, S.-W.; Tay, D. K.; Zhang, S.; So, K.-F.; Schneider, G. E. *Proc. Natl. Acad. Sci. U.S.A.* **2006**, *103*, 5054–5059.
(9) Davis, M. E.; Motion, J. M.; Narmoneva, D. A.; Takahashi, T.; Hakuno, D.; Kamm, R. D.; Zhang, S.; Lee, R. T. *Circulation* **2005**, *111*, 442–450.
(10) Grinstaff, M. W. *Biomaterials* **2007**, *28*, 5205–5214.
(11) Mikos, A. G.; Herring, S. W.; Ochareon, P.; Elisseeff, J.; Lu, H. H.; Kandel, R.; Schoen, F. J.; Toner, M.; Mooney, D.; Atala, A.; Van Dyke, M. E.; Kaplan, D.; Vunjak-Novakovic, G. *Tissue Eng.* **2006**, *12*, 3307–3339.
(12) Peppas, N.; Bures, P.; Leobandung, W.; Ichikawa, H. *Eur. J. Pharmacol. Biopharm.* **2000**, *50*, 27–46.
(13) Hoffman, A. S. *Adv. Drug Delivery Rev.* **2002**, *43*, 3–12.
(14) Langer, R.; Peppas, N. A. *AIChE J.* **2003**, 2990–3275.
(15) Lee, K. Y.; Mooney, D. J. *Chem. Rev.* **2001**, *101*, 1869–1879.
(16) Reichert, M.; Stark, H. *Phys. Rev. E* **2004**, *69*, 031407.
(17) Lutolf, M. P.; Hubbell, J. A. *Nat. Biotechnol.* **2005**.
(18) Stevens, M. M.; George, J. H. *Science* **2005**, *310*, 1135–1138.
(19) Ozbas, B.; Rajagopal, K.; Schneider, J. P.; Pochan, D. J. *Phys. Rev. Lett.* **2004**, *93*, 268106.
(20) Veerman, C.; Rajagopal, K.; Pochan, D. J.; Schneider, J. P.; Furst, E. M. *Macromolecules* **2006**, *39*, 6608–6614.
(21) Larsen, T. H.; Furst, E. M. *Phys. Rev. Lett.* **2008**, *100*, 146001.
(22) Larsen, T. H.; Schultz, K. M. S. *Korea-Austr. Rheol. J.* **2008**, *20*, 165–173.
(23) Crocker, J. C.; Grier, D. G. *J. Colloid Interface Sci.* **1996**, *179*, 298–310.
(24) Mason, T. G.; Weitz, D. A. *Phys. Rev. Lett.* **1995**, *74*, 1250–1253.
(25) Gittes, F.; Schnurr, P.; Olmsted, F.; MacKintosh, F.; Schmidt, C. *Phys. Rev. Lett.* **1997**, *79*, 3286–3289.
(26) Palmer, A.; Xu, J.; Wirtz, D. *Rheol. Acta* **1998**, *37*, 97–106.
(27) Ferry, J. *Viscoelastic Properties of Polymers*; Wiley: New York, 1980.
(28) Winter, H. H.; Chambon, F. *J. Rheol.* **1986**, *30*, 367–382.
(29) Winter, H. H.; Mours, M. *Adv. Polym. Sci.* **1997**, *134*, 165–234.
(30) Adolf, D.; Martin, J. E. *Macromolecules* **1990**, *23*, 3700–3704.
(31) Savin, T.; Doyle, P. S. *Biophys. J.* **2005**, *88*, 623–638.
(32) Pratt, L. R. J. *Annu. Rev. Phys. Chem.* **2002**, *53*, 409–436.
(33) Hwang, W.; Marini, D. M.; Kamm, R. D.; Zhang, S. *J. Chem. Phys.* **2003**, *118*, 389–397.
(34) Israelachvili, J. M. *Intermolecular and Surface Forces*, 2nd ed.; Academic Press: San Diego, CA, 1992.
(35) Verwey, E. J.; Overbeek, J. T. G. *Theory of the Stability of Lyophobic Colloids*, 1st ed.; Dover Publications: Mineola, NY, 1948.
(36) Devereux, O. F.; de Bruyn, P. L. *Interaction of Plane Parallel Double Layers*, 1st ed.; M.I.T. Press: Cambridge, MA, 1963.
(37) Zhang, S.-M. *J. Colloid Interface Sci.* **2003**, *268*, 154–167.
(38) Zhang, S. *Surf. Rev. Lett.* **2005**, *12*, 523–537.
(39) Zhang, S. *Colloid J.* **2005**, *67*, 613–622.
(40) Russel, W. B.; Saville, D. A.; Schowalter, W. R. *Colloidal Dispersions*; Cambridge University Press: New York, 1989.
(41) Andrews, J. M.; Roberts, C. J. *J. Phys. Chem. B* **2007**, *111*, 7897–7913.